Supplementary Materials for

Two-dimensional hole gas in organic semiconductors

Naotaka Kasuya, Junto Tsurumi, Toshihiro Okamoto, Shun Watanabe‡, and Jun Takeya‡

‡ To whom correspondence should be addressed; E-mail: swatanabe@edu.k.u-tokyo.ac.jp, and takeya@k.u-tokyo.ac.jp

This PDF file includes:

A. DETAILS OF TRANSPORT MEASUREMENTS

Sample preparation

The electric double-layer transistors (EDLTs) studied in this work were fabricated on a polyethylene naphthalate (PEN) substrate. The PEN film (Teijin Ltd., Q65HA, 125 μm) was pre-baked at 150 °C for 3 h to reduce internal stress and cooled down slowly to room temperature. After cleaning the PEN film with acetone and 2-propanol in an ultrasonic bath, parylene (dix-SR, KISCO Ltd.) was coated onto the PEN film via chemical vapor deposition, achieving a thickness of 200 nm. The single-crystal bilayer C_8-DNBDT-NW[3]was grown on the parylene layer from 3-chlorothiophene with a concentration of 0.020 wt% at 70 °C via the continuous edge casting method.[2] Gold (62 nm)/chromium (8 nm) were evaporated on the parylene/PEN substrate and single-crystal C_8-DNBDT-NW through shadow masks to form the source, drain, side gate electrodes, and voltage probes. Laser etching (V-Technology Co., Ltd., Callisto (266 nm)) was carried out for the C_8-DNBDT-NW layer to form Hall bar.

The ion gel film was spin-coated onto the PEN film (Teijin Ltd., Q51, 25 μm) with a solution composed of poly(vinylidene fluoride-*co*-hexafluoropropylene)(P(VDF-HFP)), ionic liquid (1-Ethyl-3-methylimidazolium: [EMIM] and bis(trifluoromethylsulfonyl)imide: [TFSI], respectively) and, acetonitrile (1:2:10 wt. ratio). After cutting the ion gel with the PEN film, EDLTs were completed by the lamination of the ion gel and the PEN film onto the Hall bar-shaped single-crystal C_8-DNBDT-NW and side-top gate.

Transport measurement

Low-temperature magnetotransport measurements were performed at least 12 h after the EDLT sample was inserted into a He gas-exchange cryostat with a superconducting magnet. Transfer characteristics in the linear regime (at drain voltage $V_{\mathrm{D}} = -0.10$ V) were continuously recorded by a sweeping gate voltage V_{G} at a rate of 50 mV per 30 s. Introduction of the holes onto C_8-DNBDT-NW at 260 K was undertaken by applying V_{G} , for which V_{G} was negatively increased from 0 V to the target voltage at a rate of 50 mV per 30 s. When V_{G} was changed, samples were heated up to 260 K and discharged with $V_{\mathrm{G}} = 0$ V. After charging the C_8-DNBDT-NW by applying the target V_{G} at 260 K, the temperature T dependence of the sheet resistance R_{S} is measured by monitoring the drain current I_{D} and the voltage probes. Constant $V_{\mathrm{D}} = -0.10$ V is applied during the slow ramping of T downwards and upwards with the ramping rate of 0.2 K min^{-1}. Hall measurements were performed with a constant DC I_{D} (1μA). During sweeping, an external magnetic field B was applied perpendicular to the sample plane, not exceeding $\pm$10 T and with a slow sweeping rate of 0.01 T s^{-1}.

Determination of Fermi level

The observation of metallic states in single-crystal C_8-DNBDT-NW with a high carrier density exceeding 4×10^{13} cm^{-2} in this work is accompanied by Fermi degeneracy. To investigate the relationship between the carrier density n and Fermi level μ' , we estimate the Fermi level of C_8-DNBDT-NW from the following equation:

$$n = \int_{-\infty}^{\infty} D(E)\,(1 - f(E))\,dE \tag{1}$$

Where $D(E)$ is the density of states of C_8-DNBDT-NW and $f(E)$ is the Fermi distribution function $f(E) = [1 + \exp((E-\mu')/(k_{\mathrm{B}}T))]^{-1}$. The carrier density n is estimated from the Hall effect at 180 K, and is assumed to be temperature-independent at least within the temperature from 180 K to 260 K. The density of states of C_8-DNBDT-NW is calculated

using CRYSTAL 17 at the B3LYP functional and POB-DZVP basis set level.

B. SAMPLE DEPENDENCE OF TRANSPORT PROPERTIES

Sheet conductivity σ_{4T} at 260 K

Figure. B-1a and b show the reproducibility of multiple gate sweep and the sample dependence of sheet conductivity σ_{4T} at 260 K, respectively, obtained by $\sigma_{4T} = (L_{4T}/W)\,(I_D/V_{4T})$ as a function of V_G (L_{4T} is the length between four-terminal voltage probes, W is the channel width, and V_{4T} is the potential difference between four-terminal voltage probes). All measurements are performed with $V_D = -0.10$ V during V_G sweeping at a rate of 50 mV per 30 s. σ_{4T} reaches around 60 μS in all samples reproducibly, although threshold voltage depends on the samples.

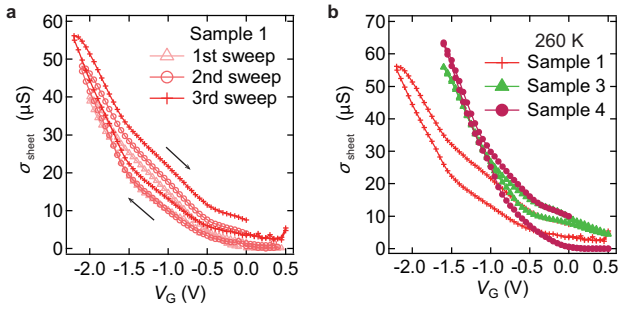

SI Fig. B-1: V_G **dependence of** σ_{4T} **at 260 K.**(a) Multiple V_G sweep in sample 1. (b) Sample dependence of σ_{4T}

Temperature dependence of sheet resistance R_S

Figure B-2 shows the temperature T dependence of sheet resistance R_S ($= {\sigma_{4T}}^{-1}$) of sample 1, 3 and 4 (the $R_S(T)$ of sample 2 is described in the main text). In sample 1, Insulator-to-metal crossover around quantum resistance h/e^2 (black dash line in the panel) is observed with negatively increasing V_G from -1.0 V to -2.2 V. The positive dR/dT is observed reproducibly for the samples 3 and 4 (Fig. B-2 b).

Hall mobility μ_{Hall} and Hall carrier density n_{Hall}

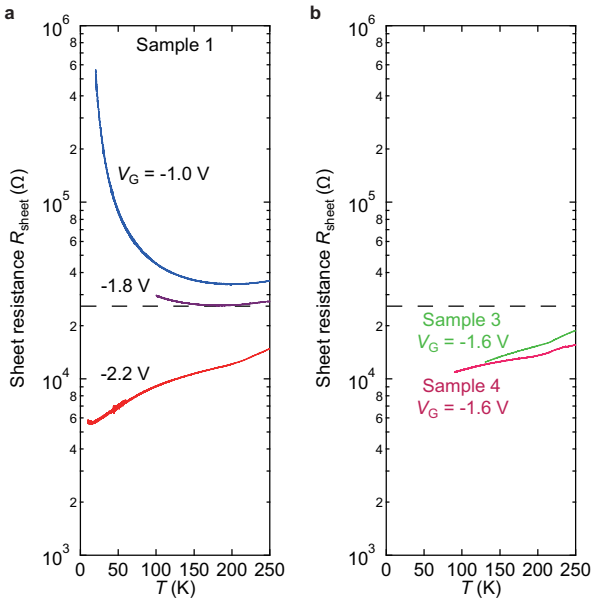

SI Fig. B-2: **The temperature dependence of sheet reisistance R_S.**

With the experimentally-obtained Hall voltage $V_{\rm Hall}$, the Hall mobility $\mu_{\rm Hall} = \sigma_{4T} R_H$ and Hall carrier density $n_{\rm Hall}$= $(eR_H)^{-1}$ are determined, in which the Hall coefficient R_H is obtained from Hall resistance R_{xy}= $V_{\rm Hall}$/ I_D= $R_H B$. For sample 1, $\mu_{\rm Hall}$ at V_G = −1.0 V decreases as temperature decreases with the activation energy E_a = 4.2 meV obtained by fitting with an Arrhenius-type thermally activated model $\mu_{\rm Hall}(T) \propto \exp(-E_a/(k_B T))$ (see the dotted curve in B-3a).

By contrast, the temperature dependence of $\mu_{\rm Hall}$ at $V_G = -2.2$ V clearly increases monotonically with a decrease in temperature (Fig. B-3a), where $\mu_{\rm Hall}$ is estimated to be 5 cm^2 V^{-1} s^{-1} at 200 K, and increases up to 25 cm^2 V^{-1} s^{-1} at 15 K. The temperature dependence of $\mu_{\rm Hall}$ can be fitted with $\mu \propto T^{-q}$ $(q > 0)$. The exponent q in the power-dependence is estimated to be $q = 0.86$. This is in a good agreement with those dominated by phonon scattering, which has been observed experimentally and theoretically for C_8-DNBDT-NW.[1] This typical metallic temperature behavior is also observed in the sample 3 at V_G= −1.6 V and sample 4 at V_G= −1.6 V (Fig.B-3b). Although the high $\mu_{\rm Hall}$ exceeding 20 cm^2 V^{-1} s^{-1} is experimentally observed at $T = 15$ K, a discrepancy in the temperature dependence of $\mu_{\rm Hall}$ from the power-law behavior is found below $T = 50$ K. This behavior is consist with a typical 2D electron/hole system, in which carrier transport is dominated by phonon scattering down to low temperatures because of few impurities in the conducting channel and then

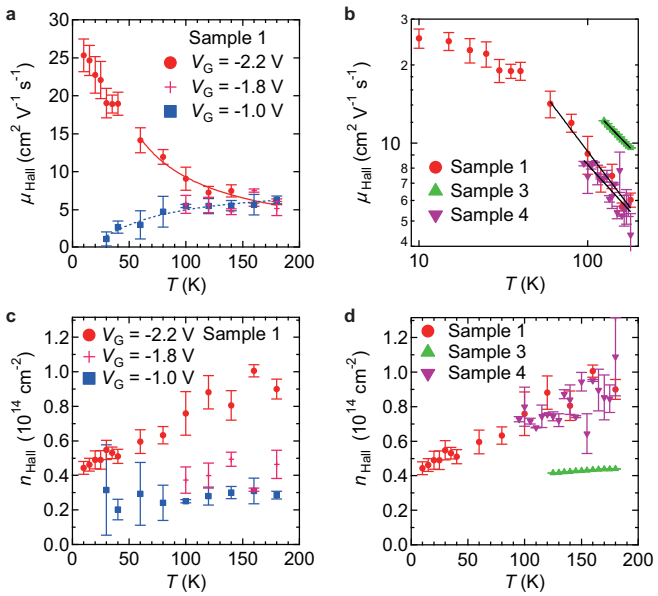

SI Fig. B-3: **The temperature dependence of Hall mobility μ_{Hall} and Hall carrier density n_{Hall}.** (a) and (c) The temperature dependence of μ_{Hall} and n_{Hall} respectively of sample 1 at various V_{G}. (b) and (d) The temperature dependence of μ_{Hall} and n_{Hall} respectively of sample 3 at $V_{\mathrm{G}}= -1.6$ V and sample 4 at $V_{\mathrm{G}}= -1.6$ V compared with that of sample 1 at $V_{\mathrm{G}}= -2.2$ V.

dominated by defect impurities scattering at cryogenic temperature, resulting in suppressing mobility.[4] The Hall carrier density n_{Hall} is estimated to be 1×10^{14} cm^{-2} at 200 K and 4×10^{13} cm^{-2} at 15 K (Fig.B-3c). Remarkably high carrier density approaching 1×10^{14} cm^{-2} at room temperature corresponds to 0.25 holes per one C_8-DNBDT-NW molecule, which is the highest carrier density observed in OSCs to the best of our knowledge, and clearly shifts the Fermi energy below the top of the valence band, which leads the Fermi degeneracy. The temperature dependence of n_{Hall} is also observed in sample 4 with $n_{\mathrm{Hall}}(180\mathrm{K}) = 1 \times 10^{14}$ cm^{-2} (Fig. B-3d).

C. MAGNEORESISTANCE OF HEAVILY DOPED C_8-DNBDT-NW

The presence of degenerated holes is further investigated through magnetotransport measurements. Figure C-1a shows the longitudinal magnetoresistance (defined as $(R(B) - R(0))/R(0)$ with respect to the application of B perpendicular to the sample plane. The positive magnetoresistance is observed over a wide temperature range, which is in a good agreement with the well-established Lorentz magnetoresistance. The characteristic phe-

nomenon that features 2D electron system is quantum galvanomagnetic effects such as Shubnikov-de Haas (SdH) effect. In general, SdH oscillation due to the quantized Landau levels is observable in sufficiently strong magnetic field, *i.e.* $\omega_c\tau = \mu B_z \gg 1$ (ω_c; the cyclotron angular momentum, τ; the momentum relaxation time). The mobilities in 2DHG in the wide-gap semiconductors are not high compared to those in 2DEG because of the high effective mass of holes in the valence band. Hence, the direct observation of SdH oscillation has not been achieved to date. On the other hand, in weak magnetic fields, the magnetotransport can be described by the semiclassical Boltzmann transport framework; the positive magnetoresistance is expected with a parabolic dependence to the applied magnetic field, *i.e.*, $(R(B) - R(0))/R(0) = {\mu_{MR}}^2 B^2$. Here, the mobility μ_{MR} is the only fitting parameter that can reproduce the magnitude of the positive magnetoresistance (shown in black curves). We summarize the temperature dependence of two mobilities determined from the Hall effect (μ_{Hall}) and longitudinal magnetoresistance (μ_{MR}) in Fig. C-1b. While the temperature dependence μ_{Hall} shows the saturation behavior as temperature decreases, which is interpreted as a crossover in hole transports from phonon scattering to ionized impurity scattering, μ_{MR} increases monotonically as temperature decreases with $\mu_{MR} \propto T^{-q}$ ($q = 0.87$). This discrepancy can be explained by the difference in scattering mechanisms.[4]

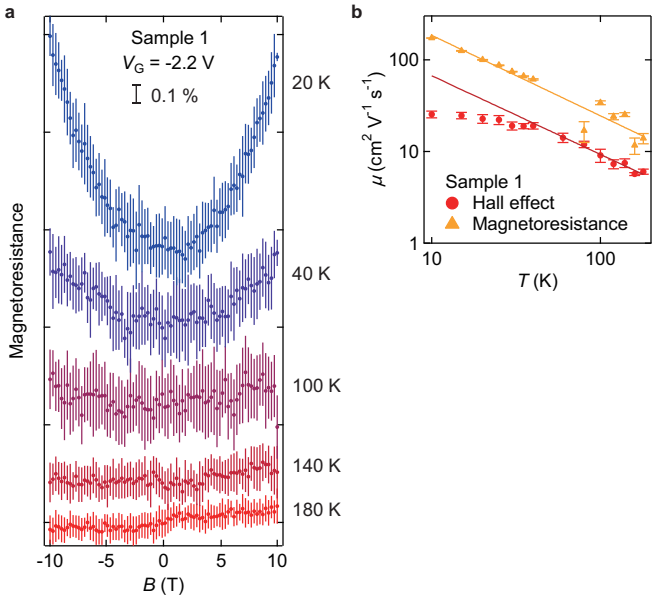

SI Fig. C-1: **The magnetoresistance of sample 1 at V_G= −2.2 V.** (a) The temperature dependence of magnetoresistance of sample 1 at V_G= −2.2 V. (b) The comparison between the Hall mobility and the mobility obtained from magnetoresistance.

A. Reference

[1] Tsurumi, J. *et al.* Coexistence of ultra-long spin relaxation time and coherent charge transport in organic single-crystal semiconductors. *Nature Physics* **13**, 994–998 (2017).

[2] Soeda, J. *et al.* Inch-size solution-processed single-crystalline films of high-mobility organic semiconductors. *Applied Physics Express* **6**, 076503 (2013).

[3] Yamamura, A. *et al.* Wafer-scale, layer-controlled organic single crystals for high-speed circuit operation. *Science Advances* **4**, eaao5758 (2018).

[4] Davies, J. H. *The Physics of Low-Dimensional Semiconductors*, 290–366 (Cambridge University Press, New York, NY, USA, 1998).